

## de Sitter space with generalized Poincaré lens

Wen Xiao,<sup>1,2</sup> Pengfei Zhao,<sup>1,2</sup> Yixiao Ge,<sup>1,2</sup> Sicen Tao,<sup>1,2</sup> Yali Zeng,<sup>1,2</sup> Lin Xu<sup>①,3</sup> and Huanyang Chen<sup>①,2,\*</sup>

<sup>1</sup>*Institute of Electromagnetics and Acoustics and Department of Physics,  
College of Physical Science and Technology, Xiamen University, Xiamen 361005, China*

<sup>2</sup>*Shenzhen Research Institute of Xiamen University, Shenzhen 518000, China*

<sup>3</sup>*Information Materials and Intelligent Sensing Laboratory of Anhui Province & Institutes of Physical Science and Information Technology, Anhui University, Hefei 230601, China*



(Received 1 April 2022; accepted 28 June 2022; published 12 July 2022)

de Sitter space is an important maximally symmetric vacuum solution of Einstein's field equation, located in a central place in cosmology in explaining the accelerated expansion of the Universe. Here in the view of optics, we propose the de Sitter space with a generalized Poincaré lens based on the equivalence between the static curved space-time and the isotropic optical medium. The correspondence of familiar de Sitter space and the Poincaré disk can be regarded as a special case therein. We also discover that the generalized de Sitter space has a topological cosmic string kernel in the center which can deflect light in different ways. This feature can be evidenced and visualized in its equivalent generalized Poincaré lens with a tunable horizon. To gain more intrinsic understanding, we further introduce its one-dimensional lens. Finally, for a possible application, we implement a multiple source illusion effect in the generalized Poincaré lens and find that the energy flow obeys the topological Poincaré-Hopf theorem. Our work is an attempt in the fruitful interplay between optics and general relativity and may enlighten other interesting relevant explorations.

DOI: [10.1103/PhysRevD.106.023507](https://doi.org/10.1103/PhysRevD.106.023507)

### I. INTRODUCTION

The past decades have witnessed great efforts to simulate the gravitational phenomena in diverse physical systems [1,2]. This strategy has made progress; for instance, the predicted Hawking radiation has been observed under existing laboratory conditions although it has yet to be evidenced by the real black holes [3–6]. In optics, the transformation optics theory [7–9] has been widely used in the analogy of general relativity. Elaborated electromagnetic materials are designed to play the role of “curved,” and the effects are visualized by the evolution of electromagnetic fields [10]. For instance, the Schwarzschild black hole with the equivalent permittivity tensor was theoretically derived and simulated [11]. The Minkowski space-time and the metric signature transition were studied in the hyperbolic metamaterials by regarding the direction of negative permittivity as the time coordinate [12]. The cosmic string of one-dimensional (1D) topological defect with robust deflection angle was constructed by multilayered rotational metasurfaces [13]. The interactions between dark matter and black hole in three typical cases were considered in both ray and wave simulations [14]. Other interesting topics, such as time travel [15], Milne universe

[16], and wormhole [17], were also investigated. To be fair, most of them require complicated anisotropic materials, which may hinder the experimental testing and realization. Remarkably, several methods that transform the curved space-time into an isotropic refractive index profile were reported [18,19], which have been successfully used to mimic the Einstein's ring [20], Kerr-Newman black hole [21] and Schwarzschild precession [22]. More intriguingly, it has been proven that the Poincaré disk of hyperbolic geometry and Maxwell's fisheye lens of spherical geometry can mimic the de Sitter and anti-de Sitter space, respectively [23], which vividly evidences some opposite features in these two space-times from the perspective of optics. It should be noted that the importance of de Sitter and anti-de Sitter space in contemporary physics is gradually increasing, for example the de Sitter model is consistent with the observed accelerated expansion of the Universe in cosmology, and the so-called AdS/CFT correspondence also indicates the vital role for anti-de Sitter space in theoretical physics [24]. As Maxwell's fisheye lens for the anti-de Sitter space has been widely studied and contributes a broad range of optical applications [25–28], the Poincaré disk for the de Sitter space ought to receive more attention in optics.

The Poincaré disk is known as an important mathematical model of hyperbolic geometry with a constant negative Gaussian curvature [29,30]. In fact, it attracts a lot of attention going beyond mathematics. The cosmological

\*Corresponding author.  
kenyon@xmu.edu.cn

alpha-attractor models in supergravity are based on the hyperbolic geometry of the Poincaré disk [31,32]. The quantum dynamics on the Poincaré disk has also been a long theoretical interest, for example the Aharonov-Bohm effect [33], the scattering problem [34], and point correlation [35]. Moreover, the motions in the Poincaré disk are used to study the optical multilayer dielectric transmission as an aspect of geometrical interpretation [36,37]. Currently, the Bloch band theory is also introduced into the Poincaré disk in which the neighboring lattices are embedded with an equal hyperbolic distance [38,39].

In this work, we propose the generalized Poincaré lens as a general version of the Poincaré disk. This is inspired from the relationship between the Maxwell fisheye lens and the generalized Maxwell's fisheye lens [40]. Based on the inverse transformation between the static curved space-time and the isotropic optical medium, we propose the corresponding generalized de Sitter space of the generalized Poincaré lens. We find that the generalized de Sitter space has a cosmic string in the center, meaning that light will be deflected due to the central conical space structure. The deflection angle depends on the topological defect of the central string, which can be vividly visualized in its equivalent generalized Poincaré lens. Light in that planar lens is observed to be repelled/attracted by the central negative/positive topological defect, where the repelled light creates a prohibited light region while the attracted light forms a self-interference light region. Furthermore, using exponential mapping  $\omega = \exp(z)$ , we obtain the 1D form of the generalized Poincaré lens. The ahead phenomena can be well understood in this 1D lens due to the cosmological event horizon scaling. As an application, we implement a multiple source illusion effect in the generalized Poincaré lens. The distribution of Poynting vector field in that effect obeys the Poincaré-Hopf theorem [41], revealing the topology nature in the unit disk. Our findings enlarge the vision of the Poincaré lens with hyperbolic geometry from mathematics and astronomy to optics, and may enlighten other interesting relevant optical applications.

## II. RESULTS AND DISCUSSION

In Ref. [23], it is pointed out that the isotropic refractive indices of the Poincaré disk  $n(r) = \frac{2}{1-r^2}$  and Maxwell's fisheye lens  $n(r) = \frac{2}{1+r^2}$  are equivalent to the static de Sitter and anti-de Sitter space. This is consistent with their optical metrics, indicating that the optical reference geometry of de Sitter space is of hyperbolic geometry with negative constant Gaussian curvature, while the anti-de Sitter space is of spherical geometry with positive curvature. On the other hand, in optics, the Maxwell's fisheye lens derives its general form, i.e. the generalized Maxwell's fisheye lens  $n(r) = \frac{2}{r^{1-m} + r^{1+m}}$ . The spherical surface is known as the geodesic lens of Maxwell's fisheye lens which can be deduced by conformal coordinate transformation [42] or

stereographic projection [43], while the shape of the geodesic lens of the generalized Maxwell fisheye lens is more common [44]. It is homeomorphic to the sphere, but also has the positive constant Gaussian curvature. Both of them have been extensively studied in optics and have brought about a series of applications in imaging, antenna, waveguide crossing. Inspired from these, we propose the "generalized Poincaré lens" with the profile  $n(r) = \frac{2}{r^{1-m} - r^{1+m}}$  ( $m \in \mathcal{Q}$  and  $m > 0$ ) to be the general version of the Poincaré disk, which differs from the generalized Maxwell fisheye lens by a minus sign in the mathematical form. Obviously, like the Poincaré disk, the generalized Poincaré lens also belongs to the hyperbolic geometry, but its physics should be much richer. Here we will focus on the optical properties of the generalized Poincaré lens. Nevertheless, we hope to explore it from the perspective of the combination of astronomy and optics. Since the Poincaré disk can be derived from the de Sitter space, it is natural to wonder what kind of curved space-time corresponds to the generalized Poincaré lens. To find such space-time, we execute the inverse calculation of Refs. [18,23]. First, we write down the general static metric with

$$ds^2 = -f(R)dt^2 + \frac{1}{f(R)}dR^2 + R^2d\Omega^2. \quad (1)$$

This metric is spatially anisotropic since the extension of radial coordinate  $R$  is different from solid angle coordinate  $\Omega$  ( $d\Omega^2 = d\theta^2 + \sin^2\theta d\varphi^2$ ) due to the factor  $\frac{1}{f(R)}$ . By performing a radial mapping  $R = R(r)$ , and following the prerequisite  $\frac{dR^2/dr^2}{f(R(r))} = \frac{R^2}{r^2}$ , the metric will be converted into a spatially isotropic one:

$$ds^2 = -f(r)dt^2 + f(r)n(r)^2(dr^2 + r^2d\Omega^2), \quad (2)$$

where  $n(r) = \frac{R(r)}{r\sqrt{f(R(r))}}$ . This  $n(r)$  is exactly the equivalent refractive index profile of the metric in Eq. (1). Now we have the generalized Poincaré lens  $n(r) = \frac{2}{r^{1-m} - r^{1+m}}$ , hence the above  $R(r)$  and  $f(R)$  can be inversely derived as

$$R(r) = \frac{2mr^m}{1+r^{2m}}, \quad f(R) = m^2 - R^2. \quad (3)$$

Consequently, the corresponded curved space-time of generalized Poincaré lens is

$$ds^2 = -(m^2 - R^2)dt^2 + \frac{1}{(m^2 - R^2)}dR^2 + R^2d\Omega^2. \quad (4)$$

We call Eq. (4) the generalized de Sitter space. Its cosmological event horizon lies at  $R = m$ . When  $m = 1$ , it goes back to the de Sitter space with the horizon of  $R = 1$ , and the equivalent lens is the familiar Poincaré disk [23]. Notably, after the radial mapping  $R(r)$  in Eq. (3), the

cosmological event horizon of the generalized de Sitter space is transformed into  $r = 1$ , which is independent of  $m$ . In addition, the static metric of de Sitter space is often used to describe the universe within the horizon, and so is the generalized de Sitter space. Therefore, in all the equivalent generalized Poincaré lenses, we only pay attention to the region within the unit disk of  $r = 1$ . Outside the unit disk it can be seen that the refractive indices become negative. When inspecting the central space-time of the generalized de Sitter space, i.e., when  $r \rightarrow 0$ , we find that the metric becomes

$$ds^2 = -m^2 dt^2 + \frac{1}{m^2} dR^2 + R^2 d\Omega^2. \quad (5)$$

Let  $R' = \frac{1}{m}R$ , Eq. (5) further transforms to  $ds^2 = -m^2 dt^2 + dR'^2 + m^2 R'^2 d\Omega^2$ . Then, following a cylindrical coordinate transformation  $z = R' \cos \theta$ ,  $\rho = R' \sin \theta$ , and without loss of generality, we set  $\theta = \frac{\pi}{2}$ , the metric will eventually settle down in the form of

$$ds^2 = -m^2 dt^2 + d\rho^2 + m^2 \rho^2 d\varphi^2 + dz^2. \quad (6)$$

By adjusting the scale of time variable  $t$ , Eq. (6) is the metric of 1D cylindrically symmetric gauge cosmic string regarding the topological defect parameter  $m$  [45,46]. It means that the generalized de Sitter space has a kernel of cosmic string with a conical space structure in the center. In a pure cosmic string, light is deflected by the central topological defect, and the behaviors can be divided into three cases [13,47–49]: when  $m > 1$ , light is repelled by the negative topological defect; when  $0 < m < 1$ , it is attracted by the positive topological defect; and when  $m = 1$ , it goes straightly with an absent defect. Hence, in the generalized de Sitter space, the light is supposed to be affected by the cosmic string especially when passing by the center. The equivalent generalized Poincaré lens will inherit this feature, thus the effect in the curved space-time can be visualized via light evolution in the unit disk of the generalized Poincaré lens. As a rotationally symmetrical refractive index distribution, the exact light ray solution in the generalized Poincaré lens can be solved by the Luneburg problem [43]; it is

$$r^m + r^{-m} = -\frac{\sqrt{1+4L^2}}{L} \sin(m\theta), \quad (7)$$

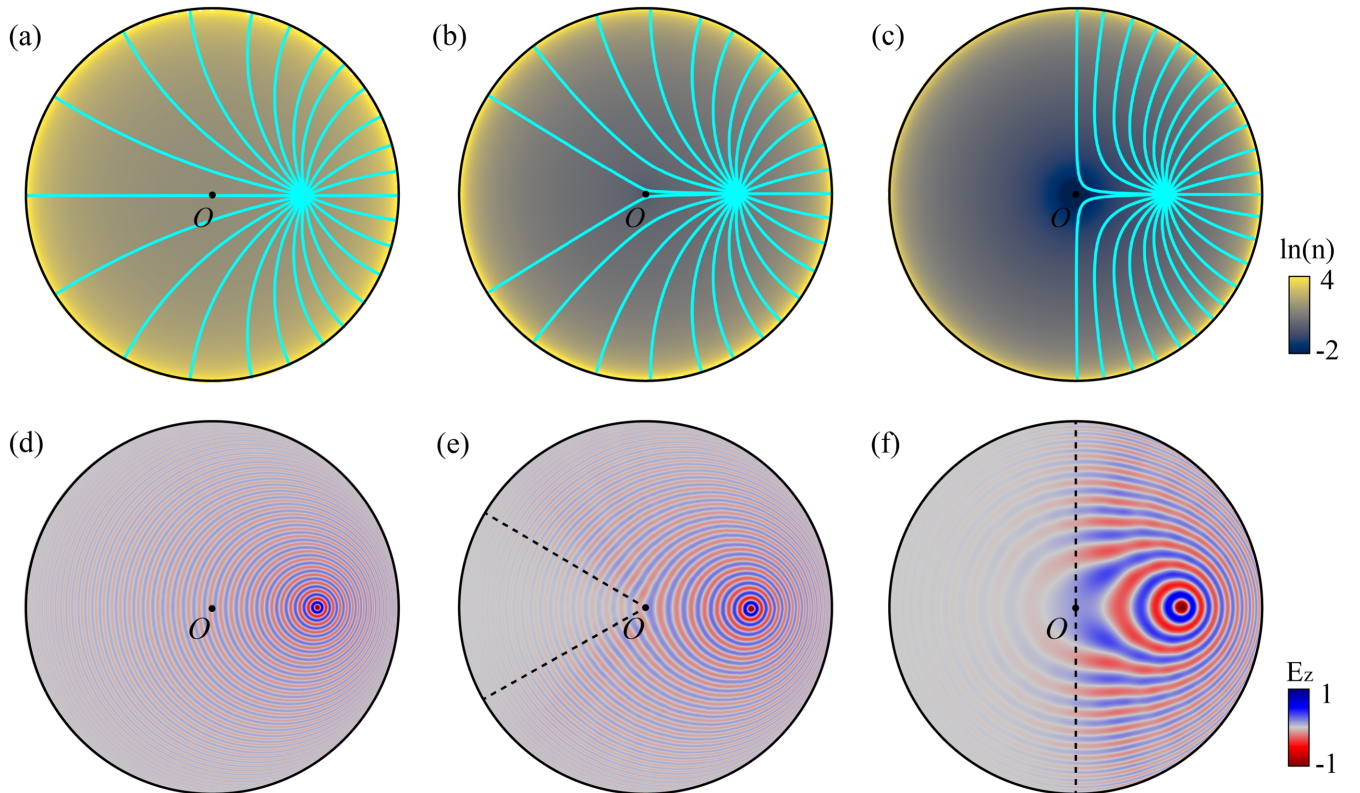


FIG. 1. Light rays and wave patterns in the unit disk of a generalized Poincaré lens with various  $m$  ( $m \geq 1$ ). Background colormaps in the rays are refractive index profiles of  $\ln(n(r))$ . (a),(d)  $m = 1$ , the familiar Poincaré disk. The refractive index equals to 2 at the origin with absent topological defect. (b),(e)  $m = \frac{6}{5}$ ; and (c),(f)  $m = 2$ . There is a zero singularity at the origin with the negative topological defect in the latter two cases. Rays and waves near the defect are repelled by the central cosmic string, resulting in a prohibited region. Range of that region: (a),(d)  $\Delta\theta = 0$ ; (b),(e)  $\Delta\theta = \frac{\pi}{3}$ ; (c),(f)  $\Delta\theta = \pi$ , respectively. The sources are all located at  $(0.5, 0)$ . Rays are satisfied with Eq. (7). The operating frequency in wave simulation of the  $E_z$  field is set as 3 GHz.

where  $L$  is the angular momentum of the ray ( $L = n_0 r_0 \sin \varphi$ ,  $\varphi$  is the tangential angle to the path). It will help us to evidence the ahead mentions.

First, we show the light propagations in the generalized Poincaré lens with various  $m$  ( $m \geq 1$ ) in Fig. 1. The familiar Poincaré disk (of  $m = 1$ ) is presented in Figs. 1(a) and 1(d). According to Eq. (7), the rays are all circular arcs and will be perpendicular to the transformed horizon (the disk boundary of  $r = 1$ ). By simply checking the refractive index, it can be found that  $n(r)$  at the origin is equal to a constant value of 2, which is indeed dovetailed with the absent topological defect when  $m = 1$ . Thus, the ray which passes the origin in the Poincaré disk will go straightly, as shown in Fig. 1(a). This also can be understood by the static metric in Eq. (5). When  $m = 1$ , the metric is the flat Minkowski space-time where the geodesic ray is always straight. The wave simulations carried by the commercial finite element software COMSOL Multiphysics agree with the geometrical rays in Fig. 1(d). Moreover, it also can be seen that since the refractive index  $n(r)$  increases monotonically with radius  $r$ , the effective wavelength at the Poincaré disk becomes smaller away from the center. As for  $m = \frac{6}{5}$  in Figs. 1(b) and 1(e), as well as  $m = 2$  in Figs. 1(c) and 1(f), light behaves quite differently. The refractive index  $n(r)$  has zero singularity at the origin when  $m > 1$ , which indicates the negative topological defect. At present, light will undergo a repulsive force when passing through the origin. In Figs. 1(b) and 1(c), the rays near the origin are repelled away in two opposite directions, then finally create an empty region that prevents light from entering. Clearly, the prohibited region edges are formed by two severely deflected rays, which are the closest to the origin and are completely governed by the central cosmic string described in Eq. (6). Although the space structure of the cosmic string is conical, despite the topological defect in the origin, it is flat with zero Gaussian curvature. Therefore, these two closest rays are nearly straight after deflection. The ranges of prohibited region can be analytically calculated through the deflection angle of the two rays (the deflection angle of cosmic string [13]), i.e.,  $\Delta\theta = \frac{2\pi(m-1)}{m}$ . In Fig. 1(b), the region is  $\Delta\theta = \frac{\pi}{3}$ ; and in Fig. 1(c), the region is  $\Delta\theta = \pi$ . The other rays that are far away from central cosmic string will not be hugely affected since the approximation is valid only when  $r \rightarrow 0$ . It is noted that all rays cannot reach the transformed event horizon  $r = 1$  since  $n(r)$  is infinite there for all the  $m$ . Because of the prohibited areas of light, the horizon ranges in the unit disk of the cases  $m = \frac{6}{5}$  and  $m = 2$  are no longer the whole circles with the full range of  $2\pi$ . For example, in Figs. 1(b) and 1(c), the ranges of horizons are  $\frac{5}{3}\pi$  and  $\pi$  at  $r = 1$ . The wave patterns in Figs. 1(e) and 1(f) are well accorded with the rays' results. The wave fronts of a line current source initially evolve several periods, then are diminished at the edges. However, the edges do not cause reflection as if the light seems to be

“topological protected.” The ability that can confine light in a certain area is expected to be useful in the beam steering system. For example, when  $m = 2$  in Fig. 1(c), light occupies half of the disk, which means that light can only radiate toward the right if we well truncate the lens to let the  $n(r)$  match with the air or other dielectrics. This is more evident when  $m$  is larger, where light is only allowed to spread in a particular direction with a very small volume, for instance,  $\frac{\pi}{2}$  of  $m = 4$ ,  $\frac{\pi}{3}$  of  $m = 6$ ,  $\frac{\pi}{4}$  of  $m = 8$  (not shown here), however carries all the energy of the source.

Let us now turn to investigate light in the generalized Poincaré lens with the positive-topological-defect cosmic string kernel  $0 < m < 1$ . We enumerate two cases of  $m = \frac{2}{3}$  and  $m = \frac{3}{4}$  in Fig. 2. At this time, the refractive index  $n(r)$  has the infinite singularity at the origin and attracts light, which distinguishes from the zero singularity in the previous case. In Figs. 2(a) and 2(b), it can be seen that the rays near the center are attracted and then deflected, where the upper rays deflect downward while the lower ones deflect upward relative to the origin. Actually, this portion of attracted light implies the double imaging effect of cosmic string. When a cosmic string is in the middle of the observer and a star, there are two images of the star as the light from the star passes by both sides of the string and reaches the observer [45]. However, the other far away rays

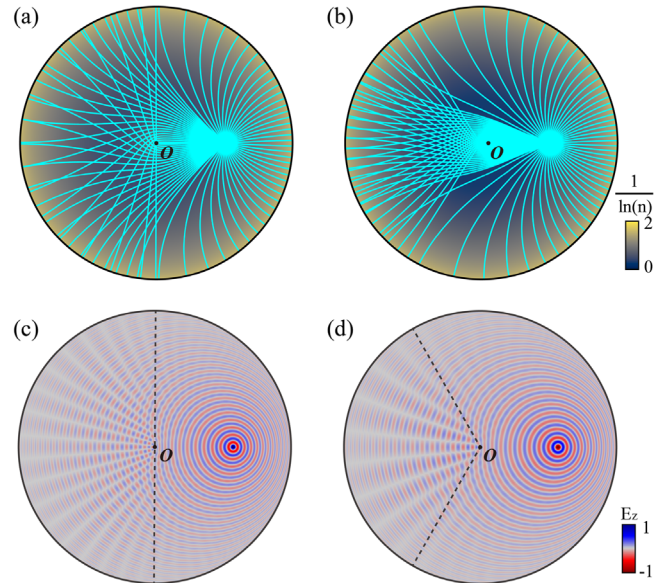


FIG. 2. Light rays and wave patterns in the unit disk of the generalized Poincaré lens with central positive topological defects ( $0 < m < 1$ ). Background colormaps in the rays indicate a refractive index profile of  $\frac{1}{\ln(n(r))}$ . (a),(c)  $m = \frac{2}{3}$ . (b),(d)  $m = \frac{3}{4}$ . The refractive index  $n(r)$  has the infinite singularity at the origin. Rays and waves near the defect are attracted by the cosmic string core in the generalized Poincaré lens, creating a self-interference region. Range of that region: (a),(c)  $\Delta\theta = \pi$  and (b),(d)  $\Delta\theta = \frac{2}{3}\pi$ , respectively. The sources are in  $(0.5, 0)$ , and the operating frequency is set as 1.5 GHz.

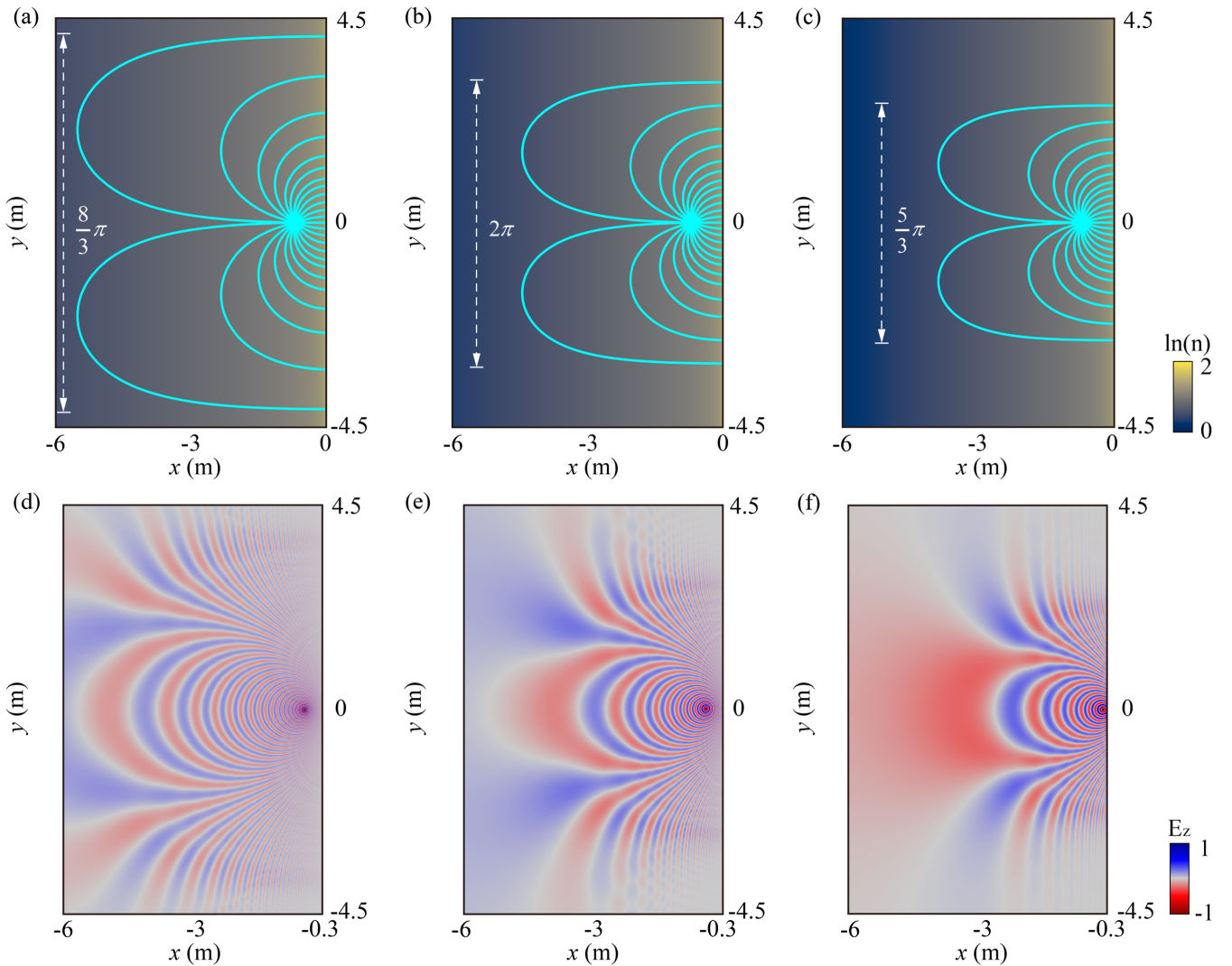


FIG. 3. Light rays and wave patterns in the 1D lens  $n(x) = -\frac{1}{\sinh mx}$ . The background colormaps in the rays show the refractive index profile  $\ln(n(r))$ . (a),(d)  $m = \frac{3}{4}$  with horizon range  $\frac{8}{3}\pi$ . (b),(e)  $m = 1$  with horizon range  $2\pi$ . (c),(f)  $m = \frac{6}{5}$  with horizon range  $\frac{5}{3}\pi$ . The sources of the rays and waves are all located at  $(\ln(0.5), 0)$ . The operating frequency is set as 3 GHz.

in the generalized Poincaré lens are keeping their path, not affected by the string. Finally, all the rays generate an obvious interlaced but not a prohibited area, where two rays closest to the origin build the edges. The interlaced rays indicate the self-interference effect in the wave patterns as shown in Figs. 2(c) and 2(d). Similarly, following the cosmic string theory, the interference region is [13]:  $\Delta\theta = \frac{2\pi(1-m)}{m}$ . Thus, when  $m = \frac{2}{3}$  in Fig. 2(a),  $\Delta\theta = \pi$  and when  $m = \frac{3}{4}$  in Fig. 2(b),  $\Delta\theta = \frac{2}{3}\pi$ . In the wave evolution of Figs. 2(c) and 2(d), the wave fronts outside the self-interference region are keeping cylindrically; once arriving in that region, they are redistributed, producing alternately dark and bright strips. This self-interference region can be customized by changing the  $m$ , and such a unique pattern in the generalized Poincaré lens with  $0 < m < 1$  may find applications in sensing and detection, since any additional scatter will destroy the field distribution. In

addition, comparing Figs. 2 and 1, we can find that the undeflected light rays behave similarly, just like those in the Poincaré disk. In other words, in terms of the radial direction, the light obeys the same rule of the de Sitter space. A similar treatment has been applied to analyze the Nariai solution of Einstein's field equation [50]. It is said that the propagation of light of the Nariai metric presents the same results with the de Sitter space when only considering the purely radial case  $d\Omega^2 = 0$  [50]. In our generalized de Sitter space, the central cosmic string can change the angular direction of light but will not have a significant impact on the radial part especially when the light is far away from the center.

The metric of the generalized de Sitter space implies the location of the event horizon and the deflection of light; however, it does not tell that the range of the horizon will also be changed. To better understand the tunable horizon in the generalized Poincaré lens, we introduce the 1D form

with a profile of  $n(x) = -\frac{1}{\sinh mx}$  through the conformal mapping  $\omega = \exp(z)$ . Previous studies have shown that the 1D lens is more instinct than its two-dimensional (2D) form [40,51]. After mapping, the unit disk is transformed into the area of  $x \in [-\infty, 0]$ , and we plot the rays and waves with several typical  $m$  in Fig. 3. It can be seen that all the rays emitted from the point source are eventually running towards the wall of  $x = 0$ . That wall is the transformed event horizon from the disk boundary, where the 1D distributed refractive index  $n(x)$  is also infinite. Furthermore, in the 1D lens, the light covers a different range in the horizon wall due to different  $m$ . They are measured as  $\frac{8}{3}\pi$  of  $m = \frac{3}{4}$  in Fig. 3(a),  $2\pi$  of  $m = 1$  in Fig. 3(b), and  $\frac{5}{3}\pi$  of  $m = \frac{6}{5}$  in Fig. 3(c). Interesting, the horizon ranges of the latter two cases are actually equal to those in the 2D lenses [see Figs. 1(a) and 1(c)]. These various horizon ranges can be attributed to the  $m$ , namely, they can be regarded as rescaled in the form of  $\frac{2\pi}{m}$ . When  $m > 1$ , the horizon is less than  $2\pi$ , and therefore in the 2D generalized Poincaré lens there is an empty range of  $2\pi(1 - \frac{1}{m})$  which avoids light arriving. Accordingly, the horizon will be larger than  $2\pi$  when  $m < 1$ . As the maximum range of the unit disk is only  $2\pi$ , the extra range will get folded, resulting the interlaced rays and the self-interference wave pattern. However, the self-interference will not occur in the 1D lens since the light range can be freely tuned along the longitudinal direction. In addition, it is already known that the rays are perpendicular to the circular horizon in the Poincaré disk, hence in its corresponded 1D lens of  $m = 1$ , the rays are also perpendicular to the horizon wall. Since rescaling only changes the horizon range, therefore, in the 1D case, the rays will be perpendicular to the horizon wall. This also indicates that in the generalized Poincaré lens, no matter what  $m$  is, all the rays are eventually perpendicular to the circle of  $r = 1$  too. Meanwhile, it further verifies the previous discussion that if only considering the propagation of light in the radial direction, the generalized de Sitter space and the conventional de Sitter space will give the same results. Figures 3(d)–3(f) are the wave simulations in the 1D lenses; their patterns are consistent with the rays. Although there is a finite horizon range in vertical direction, waves are not very sharply cut off, and its boundaries form the caustics. Such a property that light can be bound to a specific 1D range free of the source location and wavelength is useful in the lighting design. Imagine that light sources of different frequencies can work in it at the same time, showing different colors in different locations, as long as the geometrical optics approximation is satisfied. It is worth noting that the 1D lens is also hyperbolic since conformal mapping will not change the inherent topology; thus this lens may also serve as a complementary platform for studying hyperbolic geometry.

Based on the above optical properties, here we implement a multiple source illusion effect in the generalized Poincaré lens. In Fig. 2, it is noticed that the double images of source can be observed in some area of the generalized Poincaré lens, due to the attraction of the central cosmic

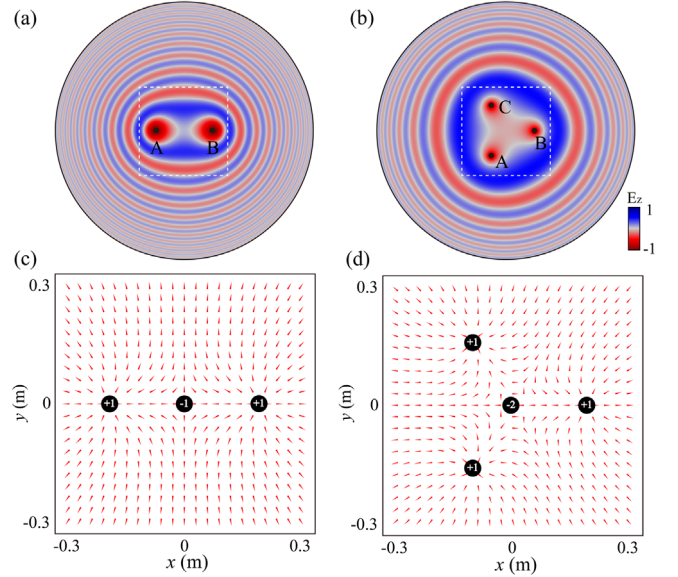


FIG. 4. Illusion effect in the generalized Poincaré lens, operating frequency is set as 3 GHz. (a) Illusion with two sources when  $m = 2$ . The source positions are at  $A(-0.2, 0)$  and  $B(0.2, 0)$ . (b) Illusion with three sources when  $m = 3$ . The sources are at  $A(-0.1, -0.1\sqrt{3})$ ,  $B(0.2, 0)$ , and  $C(-0.1, 0.1\sqrt{3})$ . (c),(d) The Poynting vector distribution extracted from the white box in (a) and (b). A, B or C is the isolate source in the vector field with index  $+1$  respectively. The origins are the saddle points. In (c), the origin is a simple cross saddle with index  $-1$  and in (d) it is a double cross saddle with index  $-2$ . The sum of the indices in (c) or (d) is 1, the Euler characteristic of the unit disk.

string with positive topological effect. Now, we turn to find the application of the repulsive case when  $m > 1$ . For an integer  $m$ , a light source can only illuminate the certain area of the unit disk, i.e.,  $\frac{2\pi}{m}$ . The other area is prohibited. If we carefully place  $m$  sources into the generalized Poincaré lens, the entire disk will be uniformly illuminated. Such a scene looks like only one light source (the intensity times  $m$ ) is placed in the center of the disk. Therefore, the result of multiple sources illusion is to create a virtual light source in the origin. Figure 4 demonstrates the two sources and three sources illusion effect. When  $m = 2$  in Fig. 4(a), the field radiated from one source  $A(-0.2, 0)$  or  $B(0.2, 0)$  can only account for half disk, while two sources working together will form a full cylindrical wave front. A similar trick can be done in the case of  $m = 3$  in Fig. 4(b), where the sources are located in the vertices of an equilateral triangle. We inspect their energy flow and discover that the distribution of Poynting vector field obeys the Poincaré-Hopf theorem [41], which is to say, the index of the singularities in the Poynting vector field sum over the lens is always 1 (the Euler characteristic of the unit disk). The extracted vector distributions are shown in the Figs. 4(c) and 4(d) for  $m = 2$  and  $m = 3$  respectively. The index for every real isolate source like A, B or C is marked with  $+1$ . However, in the

origin, the virtual source is equipped with saddle-shaped singularity with the negative index. In Fig. 4(c) the saddle is a simple cross point marked with index  $-1$ , while in Fig. 4(d), it is a double cross point with index  $-2$ . Hence for all cases, the sum of singularity index over the generalized Poincaré lens always remains 1. The topological Poincaré-Hopf theorem has been studied in optics to explain some important optical phenomena, for instance, the electromagnetic multipoles and the formation of bound states in the continuum [52]. Here we utilize the theorem to deal with the energy distribution in the real space, and it also can be applied to explain other optical illusion effects [49,53].

### III. CONCLUSION

In summary, we propose the generalized de Sitter space and generalized Poincaré lens as the general version of de Sitter space and Poincaré disk. By analyzing the metric, we find that the generalized de Sitter space has a kernel of 1D cosmic string, which implies that light will be deflected by the topological defect in such curved space-time. However, when considering the purely radial case, the generalized de Sitter space will give the same results as the de Sitter space. The same radial analysis was also used in the Nariai solution of Einstein's field [50]. These inferences of generalized de Sitter space are evidenced and visualized in the equivalent generalized Poincaré lens. For the negative topological defect, light creates a prohibited region and confines itself to a finite area with a tunable horizon. For the positive topological defect, light can propagate throughout the entire lens, and generates a specific self-interference region. All the light rays will be perpendicular to the horizon no matter what the topological defect is. To gain an instinctive view, the 1D type of the generalized Poincaré lens is introduced and the phenomena can be interpreted by the horizon rescaling. The unique properties of the generalized Poincaré lens and its

1D lens can be used in beam steering, detection and lighting design. We also implement an interesting multiple source illusion effect of the lens, where the Poynting vector naturally obeys the Poincaré-Hopf theorem. Although there are extreme values of zero and infinite singularities in the refractive index distribution of the generalized Poincaré lens, it can be well solved by transmuted singularity [54] and truncating lens [55], or utilizing its geodesic lens [56]. Moreover, all the new optical lenses proposed here belong to the category of hyperbolic geometry, demonstrating the great potentials of manipulating light in non-Euclidean manifolds, which is essentially different from the dispersion engineering with artificial or natural hyperbolic materials [57]. Besides, the hyperbolic band theory is attracting growing attention recently [58], and the new lattice distance metric in the generalized Poincaré lens may offer a new platform to study the band property with inherent topological defects. Indeed, optics is a powerful and fertile soil for visualizing astronomy, and it is believed that the product, the generalized Poincaré lens combining these two fields, will inspire other interesting works in the future.

### ACKNOWLEDGMENTS

This work is supported by the National Natural Science Foundation of China (Grants No. 92050102 and No. 11904006), the National Key Research and Development Program of China (Grant No. 2020YFA0710100), Shenzhen Science and Technology Program (Grant No. JCYJ20210324121610028), Fundamental Research Funds for the Central Universities (Grants No. 20720220033 and No. 20720200074), and the National Science Foundation of Anhui Province of China (Grant No. 1908085QA20). W. X. acknowledges China Scholarship Council for financial support.

- 
- [1] C. Barcelo, S. Liberati, and M. Visser, Analogue gravity, *Living Rev. Relativity* **14**, 3 (2011).
  - [2] *Analogue Gravity Phenomenology: Analogue Spacetimes and Horizons, from Theory to Experiment*, edited by D. Faccio, F. Belgiorno, S. Cacciatori, V. Gorini, S. Liberati, and U. Moschella (Springer, Cham, 2013).
  - [3] W. G. Unruh, Experimental Black-Hole Evaporation?, *Phys. Rev. Lett.* **46**, 1351 (1981).
  - [4] P. D. Nation, M. P. Blencowe, A. J. Rimberg, and E. Buks, Analogue Hawking Radiation in a dc-SQUID Array Transmission Line, *Phys. Rev. Lett.* **103**, 087004 (2009).
  - [5] J. Steinhauer, Observation of quantum Hawking radiation and its entanglement in an analogue black hole, *Nat. Phys.* **12**, 959 (2016).
  - [6] J. Drori, Y. Rosenberg, D. Bermudez, Y. Silberberg, and U. Leonhardt, Observation of Stimulated Hawking Radiation in an Optical Analogue, *Phys. Rev. Lett.* **122**, 010404 (2019).
  - [7] U. Leonhardt, Optical conformal mapping, *Science* **312**, 1777 (2006).
  - [8] J. B. Pendry, D. Schurig, and D. R. Smith, Controlling electromagnetic fields, *Science* **312**, 1780 (2006).
  - [9] H. Chen, C. T. Chan, and P. Sheng, Transformation optics and metamaterials, *Nat. Mater.* **9**, 387 (2010).
  - [10] U. Leonhardt and T. G. Philbin, General relativity in electrical engineering, *New J. Phys.* **8**, 247 (2006).
  - [11] H. Chen, R.-X. Miao, and M. Li, Transformation optics that mimics the system outside a Schwarzschild black hole, *Opt. Express* **18**, 15183 (2010).

- [12] I. I. Smolyaninov and E. E. Narimanov, Metric Signature Transitions in Optical Metamaterials, *Phys. Rev. Lett.* **105**, 067402 (2010).
- [13] C. Sheng, H. Liu, H. Chen, and S. Zhu, Definite photon deflections of topological defects in metasurfaces and symmetry-breaking phase transitions with material loss, *Nat. Commun.* **9**, 4271 (2018).
- [14] S. Tao, W. Xiao, and H. Chen, Light behaviors outside a black hole surrounded by dark matter, *Europhys. Lett.* **136**, 14002 (2021).
- [15] S. R. Boston, Time travel in transformation optics: Metamaterials with closed null geodesics, *Phys. Rev. D* **91**, 124035 (2015).
- [16] D. Figueiredo, F. Moraes, S. Fumeron, and B. Berche, Cosmology in the laboratory: An analogy between hyperbolic metamaterials and the Milne universe, *Phys. Rev. D* **96**, 105012 (2017).
- [17] R. Q. He, G. H. Liang, S. N. Zhu, and H. Liu, Simulation of giant tidal force of wormhole using curved optical spaces, *Phys. Rev. Research* **2**, 013237 (2020).
- [18] D. A. Genov, S. Zhang, and X. Zhang, Mimicking celestial mechanics in metamaterials, *Nat. Phys.* **5**, 687 (2009).
- [19] U. Leonhardt and T. Philbin, *Geometry and Light: The Science of Invisibility* (Dover, New York, 2010), pp. 20–27.
- [20] C. Sheng, H. Liu, Y. Wang, S. N. Zhu, and D. A. Genov, Trapping light by mimicking gravitational lensing, *Nat. Photonics* **7**, 902 (2013).
- [21] R. A. Tinguely and A. P. Turner, Optical analogues to the equatorial Kerr-Newman black hole, *Commun. Phys.* **3**, 120 (2020).
- [22] W. Xiao, S. Tao, and H. Chen, Mimicking the gravitational effect with gradient index lenses in geometrical optics, *Photonics Res.* **9**, 1197 (2021).
- [23] H. Chen, S. Tao, J. Bělník, J. Courtial, and R.-X. Miao, Transformation cosmology, *Phys. Rev. A* **102**, 023528 (2020).
- [24] U. Moschella, The de Sitter and anti-de Sitter sightseeing tour in *Einstein, 1905–2005*, edited by T. Damour, O. Darrigol, B. Duplantier, and V. Rivasseau, Progress in Mathematical Physics Vol. 47 (Birkhäuser Verlag, Basel, 2006), pp. 120–133.
- [25] U. Leonhardt, Perfect imaging without negative refraction, *New J. Phys.* **11**, 093040 (2009).
- [26] S. Li, Y. Zhou, J. Dong, X. Zhang, E. Cassan, J. Hou, C. Yang, S. Chen, D. Gao, and H. Chen, Universal multimode waveguide crossing based on transformation optics, *Optica* **5**, 1549 (2018).
- [27] S. H. Badri and M. M. Gilarlue, Maxwell’s fisheye lens as efficient power coupler between dissimilar photonic crystal waveguides, *Optik (Stuttgart)* **185**, 566 (2019).
- [28] Y. Zhou, Z. Hao, P. Zhao, and H. Chen, Solid Immersion Maxwell’s Fish-Eye Lens Without Drain, *Phys. Rev. Applied* **17**, 034039 (2022).
- [29] T. Needham, *Visual Complex Analysis* (Oxford University Press, New York, 1998), pp. 293–322.
- [30] É. Ghys, Poincaré and his disk, in *The Scientific Legacy of Poincaré*, edited by C. Éric, E. Ghys, and A. Lesne, History of Mathematics Vol. 36 (American Mathematical Society, Providence, RI, 2010), pp. 1–43.
- [31] J. J. M. Carrasco, R. Kallosh, and A. Linde, Cosmological attractors and initial conditions for inflation, *Phys. Rev. D* **92**, 063519 (2015).
- [32] J. J. M. Carrasco, R. Kallosh, A. Linde, and D. Roest, Hyperbolic geometry of cosmological attractors, *Phys. Rev. D* **92**, 041301(R) (2015).
- [33] O. Lisovyy, Aharonov-Bohm effect on the Poincaré disk, *J. Math. Phys. (N.Y.)* **48**, 052112 (2007).
- [34] A. L. de Jesus, A. C. Maioli, and A. G. M. Schmidt, Scattering in the Poincaré disk and in the Poincaré upper half-plane, *Phys. Scr.* **96**, 125264 (2021).
- [35] B. Doyon, Two-point correlation functions of scaling fields in the Dirac theory on the Poincaré disk, *Nucl. Phys.* **B675**, 607 (2003).
- [36] A. G. Barriuso, J. J. Monzón, and L. L. Sánchez-Soto, General unit-disk representation for periodic multilayers, *Opt. Lett.* **28**, 1501 (2003).
- [37] A. G. Barriuso, J. J. Monzón, L. L. Sánchez-Soto, and J. F. Cariñena, Hyperbolic reflections as fundamental building blocks for multilayer optics, *J. Opt. Soc. Am. A* **20**, 1812 (2003).
- [38] A. J. Kollar, M. Fitzpatrick, and A. A. Houck, Hyperbolic lattices in circuit quantum electrodynamics, *Nature (London)* **571**, 45 (2019).
- [39] J. Maciejko and S. Raman, Hyperbolic band theory, *Sci. Adv.* **7**, eabe9170 (2021).
- [40] H. Chen, Imaging along conformal curves, *Phys. Rev. A* **98**, 043843 (2018).
- [41] J. W. Milnor and D. W. Weaver, *Topology from the Differentiable Viewpoint* (Princeton University Press, Princeton, NJ, 1997), pp. 32–41.
- [42] M. Šarbot and T. Tyc, Spherical media and geodesic lenses in geometrical optics, *J. Opt.* **14**, 075705 (2012).
- [43] R. K. Luneburg, *Mathematical Theory of Optics* (University of California Press, Berkeley, 1964), pp. 175–180.
- [44] L. Xu, X. Wang, T. Tyc, C. Sheng, S. Zhu, H. Liu, and H. Chen, Light rays and waves on geodesic lenses, *Photonics Res.* **7**, 1266 (2019).
- [45] A. Vilenkin, Gravitational field of vacuum domain walls and strings, *Phys. Rev. D* **23**, 852 (1981).
- [46] K. Jusufi, F. Rahaman, and A. Banerjee, Semiclassical gravitational effects on the gravitational lensing in the spacetime of topological defects, *Ann. Phys. (Amsterdam)* **389**, 219 (2018).
- [47] Y. L. Zhang, X. Z. Dong, M. L. Zheng, Z. S. Zhao, and X. M. Duan, Steering electromagnetic beams with conical curvature singularities, *Opt. Lett.* **40**, 4783 (2015).
- [48] I. Fernández-Núñez and O. Bulashenko, Wave propagation in metamaterials mimicking the topology of a cosmic string, *J. Opt.* **20**, 045603 (2018).
- [49] L. Xu, R. He, K. Yao, J. M. Chen, C. Sheng, Y. Chen, G. Cai, S. Zhu, H. Liu, and H. Chen, Conformal Singularities and Topological Defects from Inverse Transformation Optics, *Phys. Rev. Applied* **11**, 034072 (2019).
- [50] H. Nariai, On a new cosmological solution of Einstein’s field equations of gravitation, *Gen. Relativ. Gravit.* **31**, 963 (1999).
- [51] H. Chen and W. Xiao, Morse lens [Invited], *Chin. Optic. Lett.* **18**, 062403 (2020), <https://opg.optica.org/col/abstract.cfm?uri=col-18-6-062403>.

- [52] W. Chen, Y. Chen, and W. Liu, Singularities and Poincaré Indices of Electromagnetic Multipoles, *Phys. Rev. Lett.* **122**, 153907 (2019).
- [53] P. Zhao, G. Cai, and H. Chen, Exact transformation optics by using electrostatics, *Sci. Bull.* **67**, 246 (2022).
- [54] T. Tyc and U. Leonhardt, Transmutation of singularities in optical instruments, *New J. Phys.* **10**, 115038 (2008).
- [55] H. Xu and Y. Shi, Metamaterial-based Maxwell's fisheye lens for multimode waveguide crossing, *Laser Photonics Rev.* **12**, 1800094 (2018).
- [56] Q. Chen, S. A. R. Horsley, N. J. G. Fonseca, T. Tyc, and O. Quevedo-Teruel, Double-layer geodesic and gradient-index lenses, *Nat. Commun.* **13**, 2354 (2022).
- [57] D. Lee, S. So, G. Hu *et al.*, Hyperbolic metamaterials: Fusing artificial structures to natural 2D materials, *eLight* **2**, 1 (2022).
- [58] I. Boettcher, P. Bienias, R. Belyansky, A. J. Kollar, and A. V. Gorshkov, Quantum simulation of hyperbolic space with circuit quantum electrodynamics: From graphs to geometry, *Phys. Rev. A* **102**, 032208 (2020).